Low pressure CO_2 hydrogenation to methanol over gold nanoparticles activated on a CeO_x/TiO_2 interface

Xiaofang Yang,[1] Shyam Kattel,[1] Sanjaya D. Senanayake,[1] J. Anibal Boscoboinik,[2] Xiaowa Nie,[3] Jesús Graciani,[4] José A. Rodriguez,[1] Ping Liu,[1] Darío J. Stacchiola[1,*] and Jingguang G. Chen[1,5,*]

[1]Chemistry Department, Brookhaven National Laboratory, Upton, NY 11973

[2]Center for Functional Nanomaterials (CFN), Brookhaven National Laboratory, Upton, NY 11973

[3]Dalian University of Technology, Dalian 116024, Liaoning Province, China

[4]Department of Physical Chemistry, University of Seville, E-41012, Seville, Spain

[5]Department of Chemical Engineering, Columbia University, NY 10027

ABSTRACT: Capture and recycling of CO_2 into valuable chemicals such as alcohols could help mitigate its emissions into the atmosphere. Due to its inert nature, the activation of CO_2 is a critical step in improving the overall reaction kinetics during its chemical conversion. Although pure gold is an inert noble metal and cannot catalyze hydrogenation reactions, it can be activated when deposited as nanoparticles on the appropriate oxide support. In this combined experimental and theoretical study, it is shown that an electronic polarization at the metal-oxide interface of Au nanoparticles anchored and stabilized on a CeO_x/TiO_2 substrate generates active centers for CO_2 adsorption and its low pressure hydrogenation, leading to a higher selectivity towards methanol. This study illustrates the importance of localized electronic properties and structure in catalysis for achieving higher alcohol selectivity from CO_2 hydrogenation.

A rising CO_2 concentration in the atmosphere has led to concerns about adverse global climate changes and ocean acidification. [1] A potential way to alleviate this problem is to capture and convert a fraction of the emitted CO_2 into inexpensive and readily available feedstock to produce chemicals or fuels. [2,3] For instance, a number of valuable chemicals can be produced from CO_2, including short-chain olefins (ethylene and propylene), syngas (CO and H_2, co-fed with methane), formic acid, methanol, dimethyl ether, and other hydrocarbons. Two of the most attractive routes involve reaction with H_2, generated from renewable sources, to convert CO_2 into CO through the reverse water gas shift (RWGS) reaction [4] and to directly synthesize methanol through further CO hydrogenation. [1,5,6]

Due to the high thermodynamic stability of CO_2, splitting of a C-O bond in the molecule is characterized by a high energy barrier. Thus, effective activation of CO_2 is a critical step in improving the overall reaction kinetics of the process. It has been proposed that activation of CO_2 occurs at the oxide support or the interfacial sites between the active metal and the oxide support. [7] Here, we will explore in detail the interaction of CO_2 with Au nanoparticles supported on CeO_x/TiO_2 using a combination of ambient-pressure X-ray photoelectron spectroscopy (AP-XPS) and calculations based on density functional theory (DFT). Metal oxides form a major category of active support materials and their capability to activate CO_2 largely depends on their basicity and reducibility. [8-14] Reduced oxides have a strong tendency to react with CO_2 or H_2O, even causing direct C-O or H-O bond scission. Thus, stabilizing the reduced states of oxides can greatly impact their surface chemistry and catalytic activity for CO_2 activation. Previous studies of the CeO_x/TiO_2 system have shown that at small coverages of ceria, the CeO_x nanoparticles at TiO_2(110) favor Ce^{3+} cations. [12,15] Meanwhile, the Ce^{3+} sites interact extensively with admetals (Pt, Cu and Au) through electronic metal–support interactions, causing high dispersion of the active metals and changing their chemical activity. [14]

While bulk gold is catalytically inert, Au nanoparticles can be very active when deposited on oxides.[16-21]. The formation of multifunctional active sites at the metal/oxide interface can impact the activity and selectivity of catalytic reactions. An example of the highly important role of the interfacial sites can be seen from a recent study of CO_2 hydrogenation over $CeO_x/Cu(111)$.[22] The interfacial sites between CeO_x and Cu provide a unique capability to stabilize a carboxylate ($CO_2^{\delta-}$) intermediate and the subsequent hydrogenation steps also become facile and are characterized by relatively small activation energies (<0.6 eV). In the study of CO_2 hydrogenation over oxide-supported Au catalysts, the nature of the supporting oxides greatly impacts the overall CO_2 conversion and the selectivity to methanol. For example, in comparing the performance of Au/CeO_2 and Au/TiO_2, Haruta found that while Au/TiO_2 was more active than Au/CeO_2, the later exhibited higher selectivity in hydrogenating CO_2 to methanol.[18] In contrast to the well-studied oxidation reactions on gold-based catalysts, the role of Au in hydrogenation reactions has not been clarified. Here we report the synergistic effect of mixed CeO_2 and TiO_2 catalysts on the stabilization and activation of Au for the selective hydrogenation of CO_2 to methanol, which occurs at very low pressures instead of the several atmospheres of hydrogen required as reported in the literature. [17] Surprisingly, Au is promoted to have similar activity and better selectivity toward methanol than the traditionally used Cu catalyst.[22] More importantly, the combined AP-XPS analysis and DFT calculations allow us to resolve details in the link between the unique surface electronic properties and the CO_2 activation mechanism at an active gold-oxide interface.

Deposition of ceria on TiO_2(110) results in the formation of well dispersed ceria dimers, where all the cerium is present as Ce^{3+}.[12,14] Figure 1 shows STM images of a CeO_x/TiO_2(110) surface before and after deposition of Au. Au nucleates preferentially on defects of TiO_2(110), but the high dispersion of ceria nanoclusters makes Au/CeO_x interfaces abundant through the surface. Previous STM studies indicate that the dispersion of Au is much

larger on CeOx/TiO_2(110) than on TiO_2(110). [12,14]After sample preparation, it was then moved to the XPS position, where both temperature programmed reaction mass spectroscopy (TPR-MS) and *in-situ* ambient pressure XPS (AP-XPS) were measured. The combination of AP-XPS and mass spectrometry provides a unique capability to study the reaction kinetics and *in-situ* characterization of the surface intermediates. For comparison we also present similar experiments with Cu nanoparticles as a reference system, since Cu-based catalysts are commercially used for the synthesis of methanol from syngas.[7]

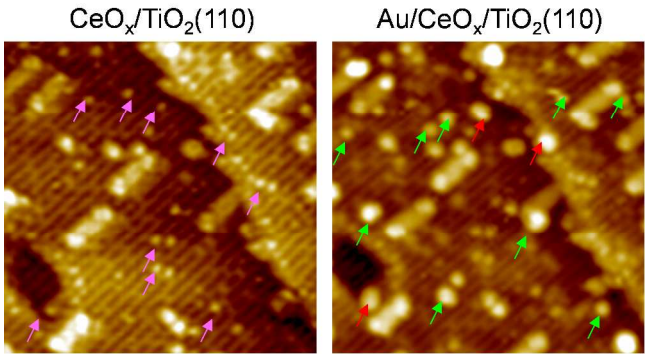

Figure 1 (Left) STM image of CeO_x/TiO_2(110) (pink arrows indicate ceria nanoparticles). (Right) STM image of $Au/CeO_x/TiO_2$(110) (Red arrows: Au near ceria; Green arrows: Au near defects of TiO_2). (Images size: 20x20 nm; V: 1.3 V and I: 0.05 nA)

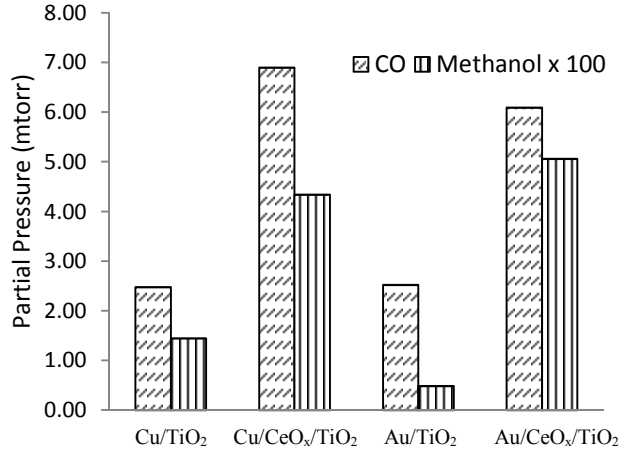

Figure 2. TPR of CO_2 hydrogenation over Cu/TiO_2 and $Cu/CeO_x/TiO_2$, Au/TiO_2 and $Au/CeO_x/TiO_2$ for producing CO and methanol. 100 mTorr CO_2 and 700 mTorr H_2 at 573 K. The partial pressures of the products at 573 K are plotted.

The TPR results of the activity and selectivity in converting CO_2 to CO and methanol are compared in Figure 2 for the surfaces of Au/TiO_2, Cu/TiO_2, $Au/CeO_x/TiO_2$ and $Cu/CeO_x/TiO_2$. No activity is found for the bare surface of either TiO_2 or CeO_x/TiO_2 (not shown). Even though bulk gold is inactive, the Au/TiO_2 surface exhibits similar activity as Cu/TiO_2 for CO production. However, the activity for methanol production is very low for the Au/TiO_2 sample. This observation is consistent with the results from Au nanoparticles on TiO_2 powders. [19] A large enhancement for methanol production is observed after adding 0.1 ML CeO_x to both surfaces. At this small coverage of CeO_x, the ceria-titania interactions are maximized and the best catalytic performance is expected.[12,14] The activity of $Au/CeO_x/TiO_2$ for methanol has been raised by one order of magnitude, comparable to that of $Cu/CeO_x/TiO_2$. The dominating reaction pathway is the RWGS reaction and the activity for CO production increases by 2-3 folds after CeO_x modification. The detection of methanol at this low hydrogen pressures (700 mTorr H_2) is unprecedented and demonstrates the potential of using $Au/CeO_x/TiO_2$ as active and selective catalysts for converting CO_2 to methanol.

To address the promoting role of CeO_x in activating CO_2 and the nature of the surface intermediates, AP-XPS of carbon-based species were measured in the presence of CO_2 and H_2 under *in-situ* reaction conditions. Figures 3A and 3B show the C1s regions after the surfaces were heated in a 100 mTorr CO_2/700 mTorr H_2 gas mixture up to 573 K and then cooled down to 323 K. The C1s spectra in Figure 3C and 3D were taken at 573 K. A peak at 284.5 eV is commonly observed during AP-XPS experiments and it is associated with adventitious carbon. The peak at ~292.8 eV is due to the gas phase CO_2. The peak at 288~290 eV is typically associated with carbonate, formate or carboxylate species ($CO_2^{\delta-}$).[22] According to similar measurements on a $CeO_x/Cu(111)$ surface, the XPS features in Figure 3 are assigned to a combination of carboxylate (~288.5 eV) species and carbonate (~289.5 eV) species at low temperatures, and co-existence of the formate (~289.2 eV) and carboxylate species at higher temperatures.[22] It is worth noting that the peak intensity of 289.6 eV is much larger on the CeO_x/TiO_2 support than on TiO_2. At 573 K, this peak on the Au/TiO_2 surface nearly disappears, but it is still visible on $Au/CeO_x/TiO_2$. Similar C1s features were observed for Cu catalysts, indicating that the surface species are most likely independent of the metallic components.

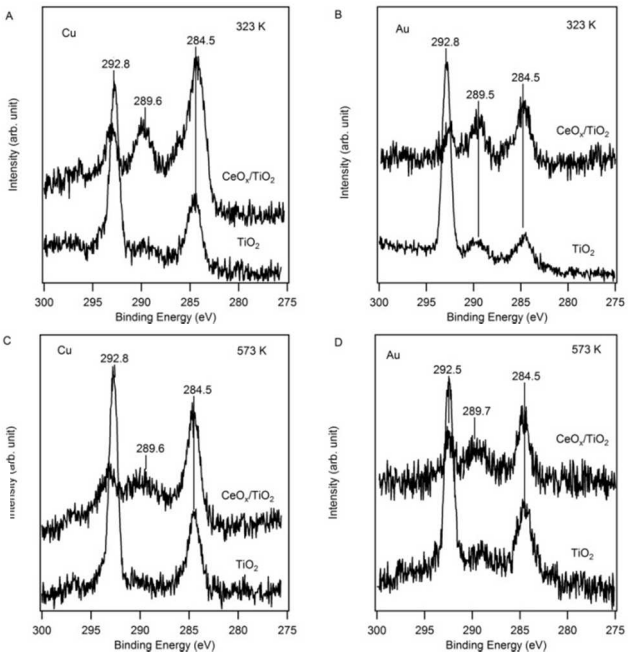

Figure 3. XPS of C1s regions measured under the presence of gases of 100 mTorr CO_2 and 700 mTorr H_2. A) and C). Cu nanoparticles; B) and D). Au nanoparticles; Spectra in A) and B) were taken at 323 K; Spectra in C) and D) were taken at 573 K. X-ray photon energy: 538 eV.

The XPS analysis of Au 4f and Ce 4d spectra provides further insights into the promoting role of CeO_x. The Au 4f spectra before reaction and under reaction conditions are compared in Figure 4A. A small shift (0.3 eV) to lower binding energy is observed for Au 4f after reaction, indicating that the Au nanoparticles were partially oxidized ($Au^{\delta+}$) before reaction and then were reduced under reaction conditions. The Ti Auger line and Ce 4d

peaks are shown in Figure 4B. The broad peak in spectrum 1 is the Ti Auger line. After depositing 0.1 ML CeO_x on TiO_2(110) under O_2, there are multiple Ce 4d peaks in spectrum 2, which are due to the spin-orbit splitting in the core level 4d and different final state effects in the 4f orbitals. [23] The peaks at 127.1 and 123.9 eV are originated from the final state without any f electron (f^0), which is the typical XPS feature of CeO_2. Thus, after CeO_x deposition in O_2, cerium is present as Ce^{4+} or mixed Ce^{4+}/Ce^{3+}. Spectrum 3 shows the Ce 4d under reaction conditions. It can be seen that the features at 127.1 and 123.9 eV disappear, indicating that all Ce^{4+} is converted into Ce^{3+}. Therefore, the activation of CO_2 requires both metallic Au and reduced Ce^{3+} and the most favorable adsorption sites are likely located at the interfacial region between Au^0 and Ce^{3+}.

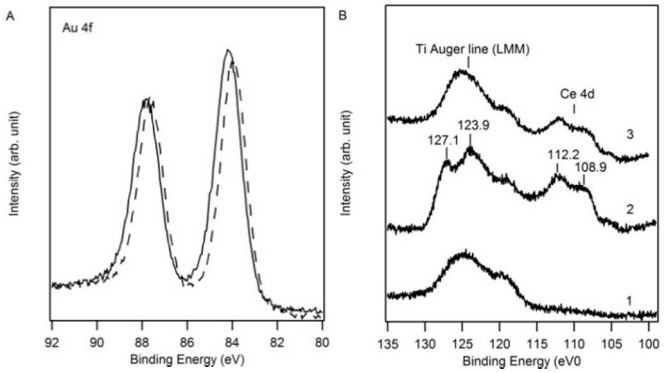

Figure 4. XPS of Au 4f and Ce 4d regions. A). Au 4f, before reaction (dash line) and after reaction (solid line), B). 1. Before depositing CeO_x, 2. After depositing CeO_x, and 3. Under reaction.

DFT calculations (see Supporting Information for details) were performed to gain a better understanding of the promoting effect of CeO_x on the catalytic activity of Au/TiO_2 observed experimentally. To this end, the TiO_2 support was modeled using a rutile TiO_2(110) surface, and CeO_x/TiO_2 mixed oxide was described by depositing Ce_2O_3 dimer on TiO_2(110) according to a previous study.[12] A gold trimer (Au_3) supported on both oxide surfaces was considered. According to DFT calculations, the Au_3 cluster is only weakly physisorbed on stoichiometric TiO_2(110) and O vacancies (O_{vac}) are required for stabilizing Au with a binding energy (BE) of -2.17 eV; in contrast the binding is stronger (BE= -2.51 eV) on a CeO_x/TiO_2(110) surface even without O_{vac}. The increased binding of Au on CeO_x/TiO_2 is attributed to the presence of Ce^{3+} cations.[15] The DFT calculations show that the Au_3 cluster binds almost on top of CeO_x supported on TiO_2(110) (Figure S4a), which is consistent with the STM measurements (Figure 1).

An electronic metal-support interaction has been considered as the origin for the enhanced oxidation activity of the supported Au nanoparticles, where the charge transfer occurs from Au to the support. [24] The current results for Au_3/TiO_2 indicate that there is a redistribution of electrons within the Au_3 unit, but the charge transfer between Au_3 and TiO_2 is essentially zero. .In the case of the Au_3-CeOx interface, the charge redistribution is significant as shown in Figure 5, while the overall charge of the Au particle remains close to zero. This is further corroborated by a density of states plot presented in Figure S2, which shows an increase in Au states near the Fermi level in $Au_3/CeO_x/TiO_2$ compared to that in Au_3/TiO_2. This unusual redistribution of electrons facilitate the strong adsorption of CO_2. The DFT results also reveal that the positively charged carbon of CO_2 tends to bind to $Au^{\delta-}$ and the negatively charged oxygen binds to $Ce^{\delta+}$.

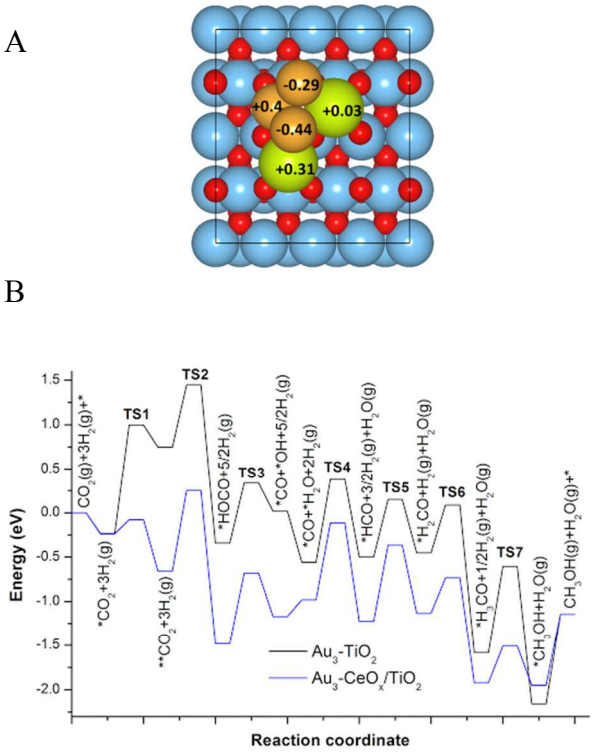

Figure 5. Charge transfer and reaction energetics calculated by DFT. A. The net Bader charges of Au and Ce. +: electron loss, -: electron gain. B. DFT-optimized potential energy surface (PES) for CO_2 hydrogenation on Au_3/TiO_2(110) and $Au_3/CeO_x/TiO_2$(110). "TS" corresponds to transition state. The corresponding geometries for each reaction intermediates were shown in Figures S3 and S4.

To determine the reaction mechanism and activity, DFT calculations were performed to optimize the potential energy surface (PES) for CO_2 hydrogenation on Au_3/TiO_2(110) and $Au_3/CeO_x/TiO_2$(110) (Figure 5). The corresponding configurations of reaction intermediates involved are shown in Figures S3 and S4. The DFT results show that the reaction occurs at the metal-oxide interface (Au/TiO_2 interface in Au nanoparticle supported on TiO_2: Figure S3, and Au/CeO_x interface in Au nanoparticle supported on CeO_x/TiO_2: Figure S4). The CO_2 hydrogenation starts with the RWGS reaction to produce CO via *HOCO intermediates on both Au_3/TiO_2(110) and $Au_3/CeO_x/TiO_2$(110), which is followed by CO hydrogenation to methanol via *HCO, *H_2CO and *H_3CO intermediates (Figure 5). On Au_3/TiO_2, the production of CO via the RWGS reaction is hindered by the relatively large activation barrier for of the activation of *CO_2 to **CO_2 (E_a = 1.65 eV), which is significantly reduced by the presence of CeO_x (E_a = 0.50 eV). All the subsequent intermediates are also stabilized by the presence of the ceria, while the barriers for their conversion remain unaltered with respect to the system without ceria. Consequently CO production should be greatly enhanced on $Au_3/CeO_x/TiO_2$ compared to Au_3/TiO_2, which is consistent with the experimental findings in Figure 2. As shown in Figures S3 and S4, Ce^{3+} of CeO_x/TiO_2(110) is much more active than Ti^{4+} of TiO_2(110) in stabilizing the tilted O of **CO_2, leading to a reduction in the corresponding barrier by 1.07 eV (Figure 5). Both CO and methanol production are promoted by the presence of CeO_x. The barrier for the last hydrogenation step, the conversion of methoxy species to methanol (TS7 in Figure 5), is also decreased by the presence of ceria, which is consistent with the improve-

ment on the selectivity to methanol observed experimentally (Figure 2).

In summary, the reduction of CO_2 by hydrogen was studied over Au/TiO_2 and $Au/CeO_x/TiO_2$ surfaces. It was found that the presence of small coverages of CeO_x (~0.1 ML) stabilizes the formation of small Au nanoparticles, significantly promoting their activity in both CO and methanol production and improving their selectivity towards methanol. The existence of carboxylate species is supported by AP-XPS under *in-situ* reaction conditions. In the $Au/CeO_x/TiO_2$ surface an electronic metal-support interaction leads to a charge redistribution in the metal near the Au-ceria interface. Such surface polarization at the metal-oxide interface promotes both CO_2 adsorption and activation. The DFT calculations further reveal that Au nanoparticles supported on the CeO_x/TiO_2 mixed oxide support decreases the reaction barriers for CO and methanol production. The interaction of CeO_x with Au nanoparticles allows this noble metal to hydrogenate CO_2 under unprecedented low pressures of hydrogen.

ASSOCIATED CONTENT

Supporting Information

Experimental details including surface preparation and characterization in UHV, kinetic study by TPR under ambient pressures and more detailed analysis of the AP-XPS data and DFT results. This material is available free of charge via the Internet at http://pubs.acs.org.

AUTHOR INFORMATION

Corresponding Author

Dr. Dario Stacchiola E-mail: djs@bnl.gov
Prof. Jingguang G. Chen E-mail: jgchen@columbia.edu

Present Addresses

Chemistry Department, Brookhaven National Laboratory (BNL) Upton, NY 11973 (USA)

Department of Chemical Engineering, Columbia University 500 W. 120th St., New York, NY 10027 (USA)

Notes

The authors declare no competing financial interests.

ACKNOWLEDGMENT

The work was sponsored under Contract No. DE-AC02-98CH10886 with the U.S. Department of Energy, Office of Science. This research used resources of the Center for Functional Nanomaterials and National Synchrotron Light Source, which are U.S. DOE Office of Science User Facilities at Brookhaven National Laboratory under Contract No. DE-SC0012704 and the National Energy Research Scientific Computing Center (NERSC) supported by the Office of Science of the US Department of Energy under Contract No. DE-AC02-05CH11231.

REFERENCES

(1) Olah, G. A.; Prakash, G. K. S.; Goeppert, A. *J. Am. Chem. Soc.* **2011**, *133*, 12881.

(2) Dorner, R. W.; Hardy, D. R.; Williams, F. W.; Willauer, H. D. *Energy Environ. Sci.* **2010**, *3*, 884.

(3) Kondratenko, E. V.; Mul, G.; Baltrusaitis, J.; Larrazabal, G. O.; Perez-Ramirez, J. *Energy Environ. Sci.* **2013**, *6*, 3112.

(4) Porosoff, M. D.; Yang, X.; Boscoboinik, J. A.; Chen, J. G. *Angew. Chem. Int. Ed.* **2014**, *53*, 6705.

(5) Rodemerck, U.; Holeňa, M.; Wagner, E.; Smejkal, Q.; Barkschat, A.; Baerns, M. *ChemCatChem* **2013**, *5*, 1948.

(6) Melaet, G.; Ralston, W. T.; Li, C.-S.; Alayoglu, S.; An, K.; Musselwhite, N.; Kalkan, B.; Somorjai, G. A. *J. Am. Chem. Soc.* **2014**, *136*, 2260.

(7) Pakhare, D.; Spivey, J. *Chem. Soc. Rev.* **2014**, *43*, 7813.

(8) Zhang, Z.; Verykios, X. *Catal. Lett.* **1996**, *38*, 175.

(9) Wang, H. Y.; Ruckenstein, E. *Appl. Catal., A* **2000**, *204*, 143.

(10) Staudt, T.; Lykhach, Y.; Tsud, N.; Skála, T. s.; Prince, K. C.; Matolín, V. r.; Libuda, J. r. *J. Phys. Chem. C* **2011**, *115*, 8716.

(11) Trovarelli, A. *Catal. Rev.* **1996**, *38*, 439.

(12) Park, J. B.; Graciani, J.; Evans, J.; Stacchiola, D.; Ma, S.; Liu, P.; Nambu, A.; Sanz, J. F.; Hrbek, J.; Rodriguez, J. A. *Proc. Natl. Acad. Sci* **2009**, *106*, 4975.

(13) Zhou, K.; Yang, Z.; Yang, S. *Chem. Mater.* **2007**, *19*, 1215.

(14) Park, J. B.; Graciani, J.; Evans, J.; Stacchiola, D.; Senanayake, S. D.; Barrio, L.; Liu, P.; Sanz, J. F.; Hrbek, J.; Rodriguez, J. A. *J. Am. Chem. Soc.* **2010**, *132*, 356.

(15) Graciani, J.; Plata, J. J.; Sanz, J. F.; Liu, P.; Rodriguez, J. A. *J. Chem. Phys.* **2010**, *131*, 104703.

(16) Haruta, M.; Yamada, N.; Kobayashi, T.; Iijima, S. *J. Catal.* **1989**, *115*, 301.

(17) Haruta, M.; Tsubota, S.; Kobayashi, T.; Kageyama, H.; Genet, M. J.; Delmon, B. *J. Catal.* **1993**, *144*, 175.

(18) Sakurai, H.; Tsubota, S.; Haruta, M. *Appl. Catal., A* **1993**, *102*, 125.

(19) Sakurai, H.; Haruta, M. *Catal. Today* **1996**, *29*, 361.

(20) Remediakis, I. N.; Lopez, N.; Nørskov, J. K. *Appl. Catal., A* **2005**, *291*, 13.

(21) Lopez, N.; Nørskov, J. K. *J. Am. Chem. Soc.* **2002**, *124*, 11262.

(22) Graciani, J.; Mudiyanselage, K.; Xu, F.; Baber, A. E.; Evans, J.; Senanayake, S. D.; Stacchiola, D. J.; Liu, P.; Hrbek, J.; Sanz, J. F.; Rodriguez, J. A. *Science* **2014**, *345*, 546.

(23) Mullins, D. R.; Overbury, S. H.; Huntley, D. R. *Surf. Sci.* **1998**, *409*, 307.

(24) Liu, X.; Liu, M.-H.; Luo, Y.-C.; Mou, C.-Y.; Lin, S. D.; Cheng, H.; Chen, J.-M.; Lee, J.-F.; Lin, T.-S. *J. Am. Chem. Soc.* **2012**, *134*, 10251.

Table of Content (TOC)

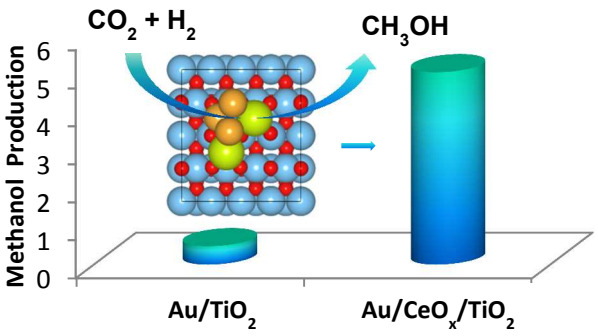

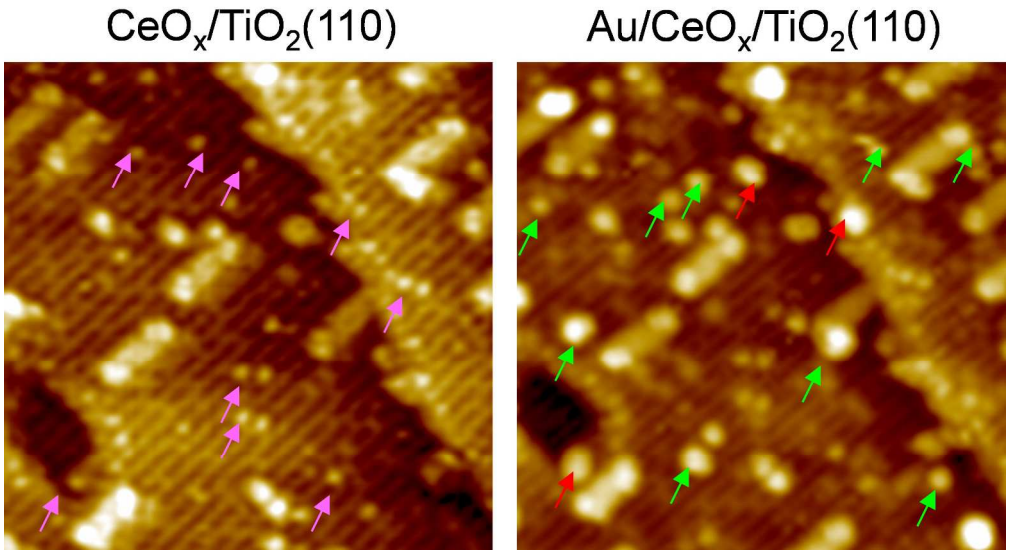

585x329mm (120 x 120 DPI)

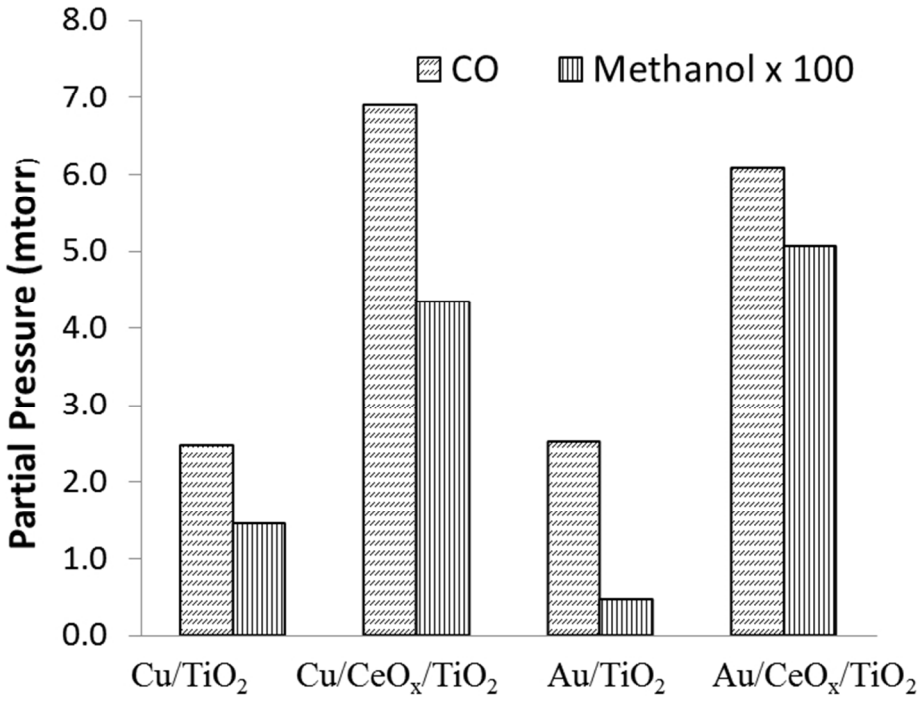
8.0
7.0
6.0
5.0
4.0
3.0
2.0
1.0
0.0
Partial Pressure (mtorr)
CO
Methanol x 100
Cu/TiO2
Cu/CeOx/TiO2
Au/TiO2
Au/CeOx/TiO2

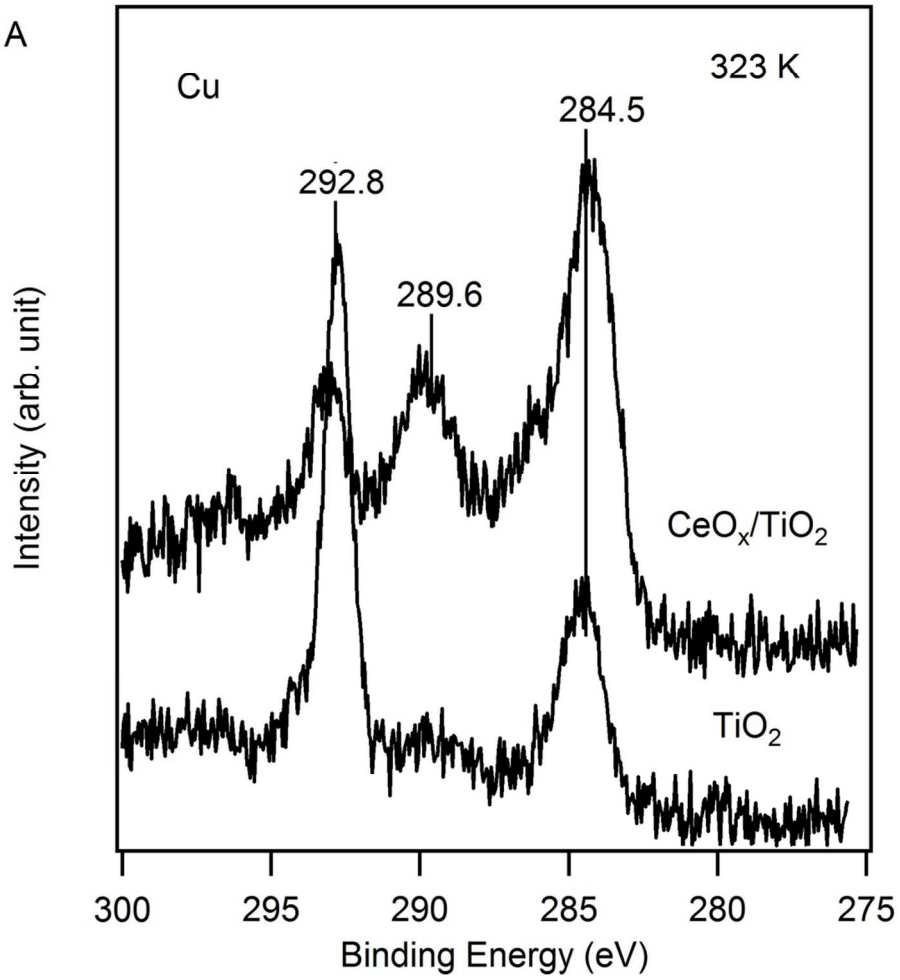

101x101mm (300 x 300 DPI)

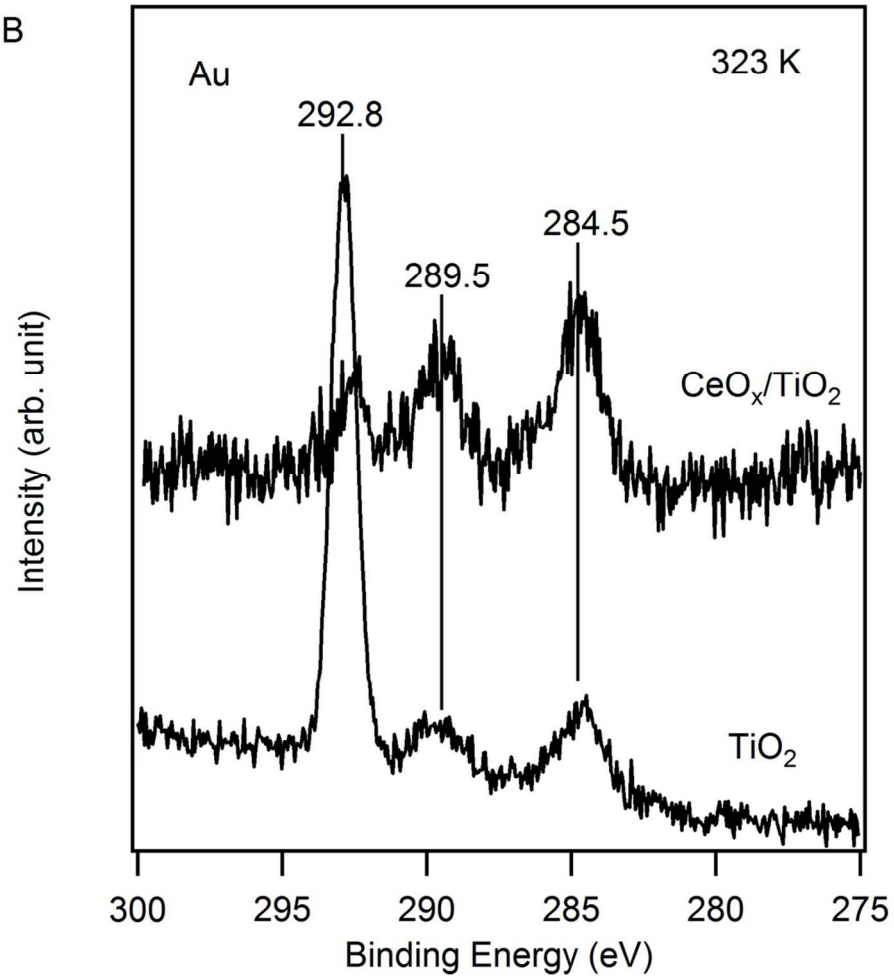

101x101mm (300 x 300 DPI)

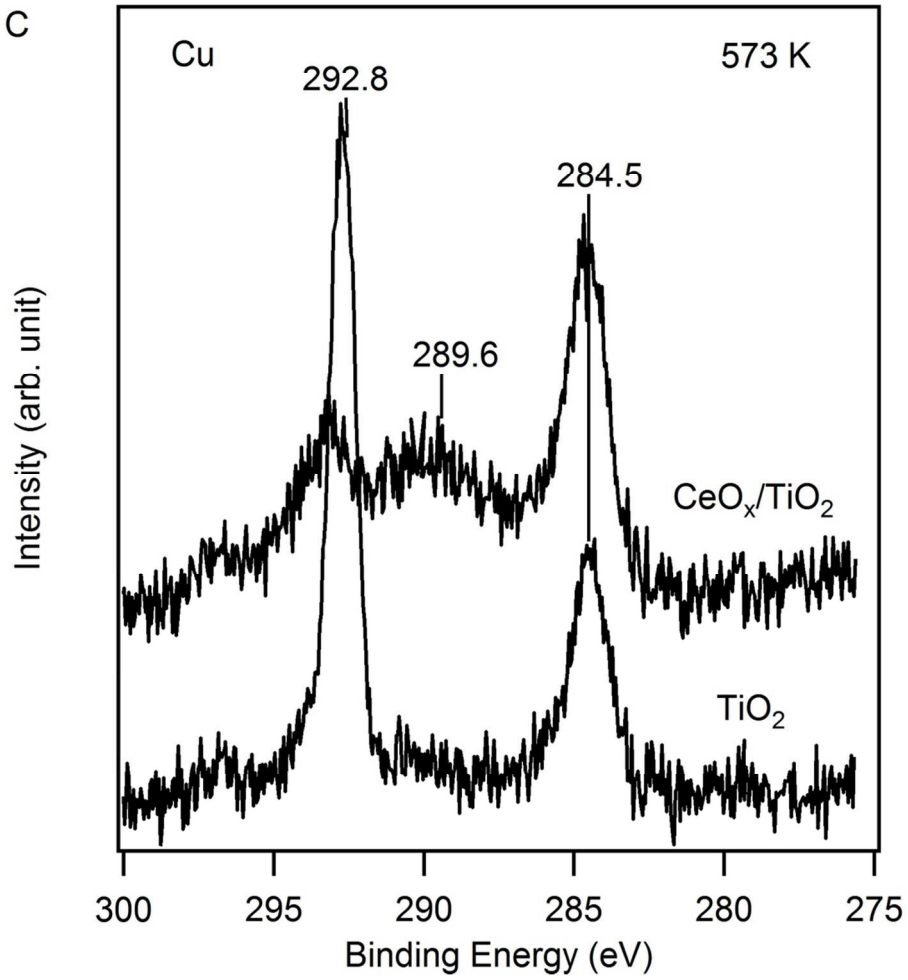

101x101mm (300 x 300 DPI)

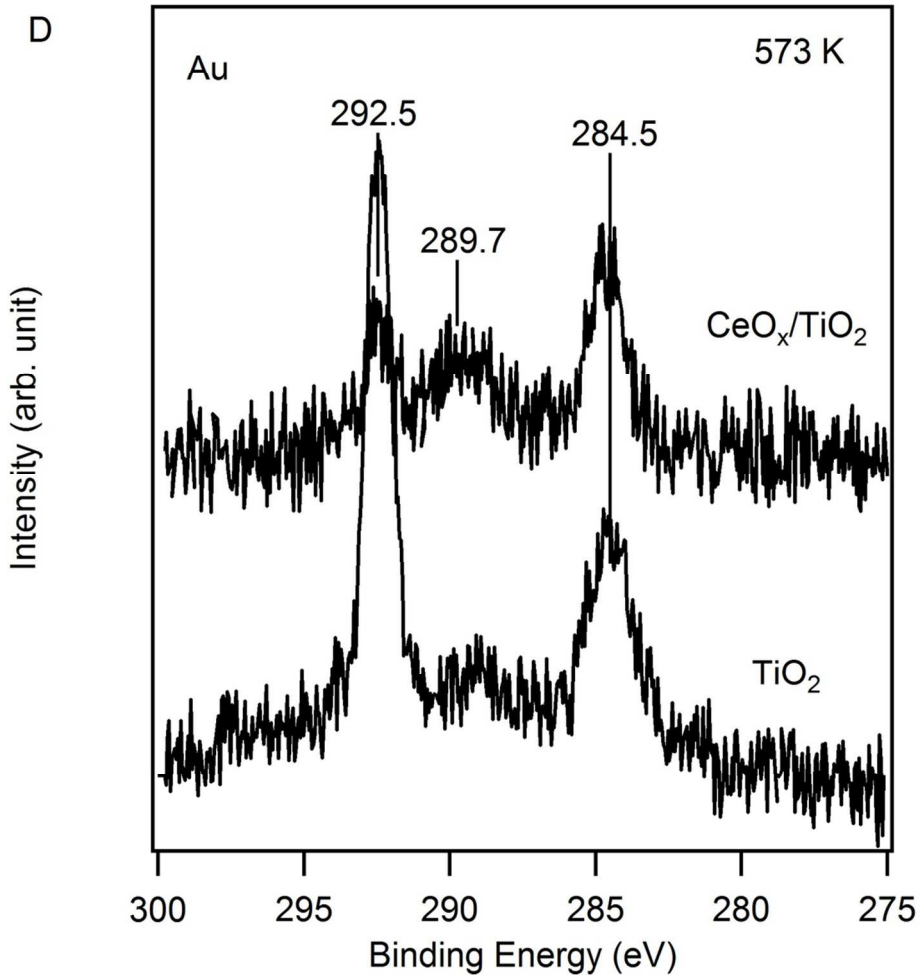

101x101mm (300 x 300 DPI)

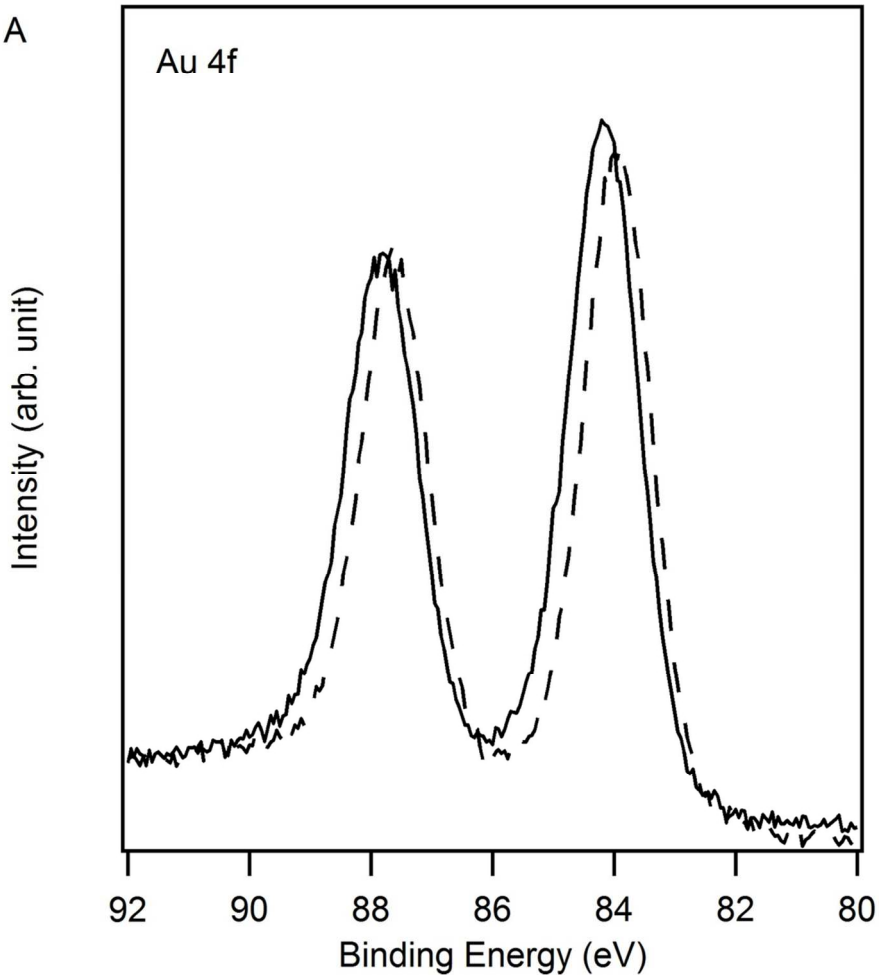

101x101mm (300 x 300 DPI)

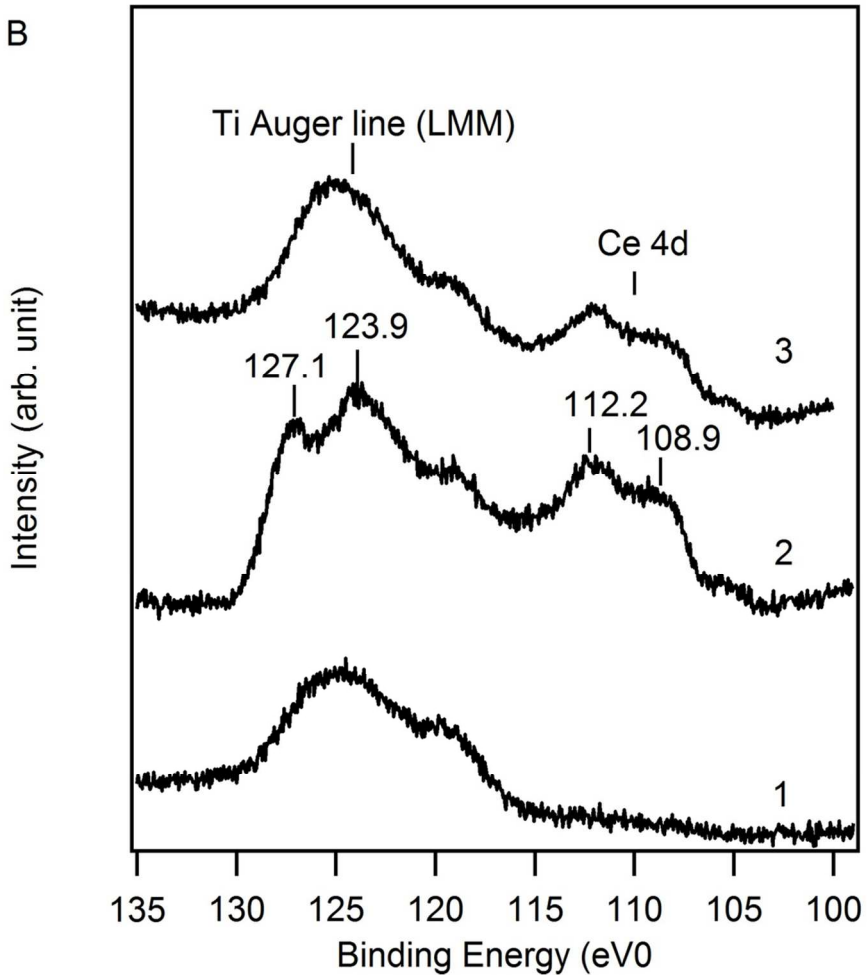

101x101mm (300 x 300 DPI)

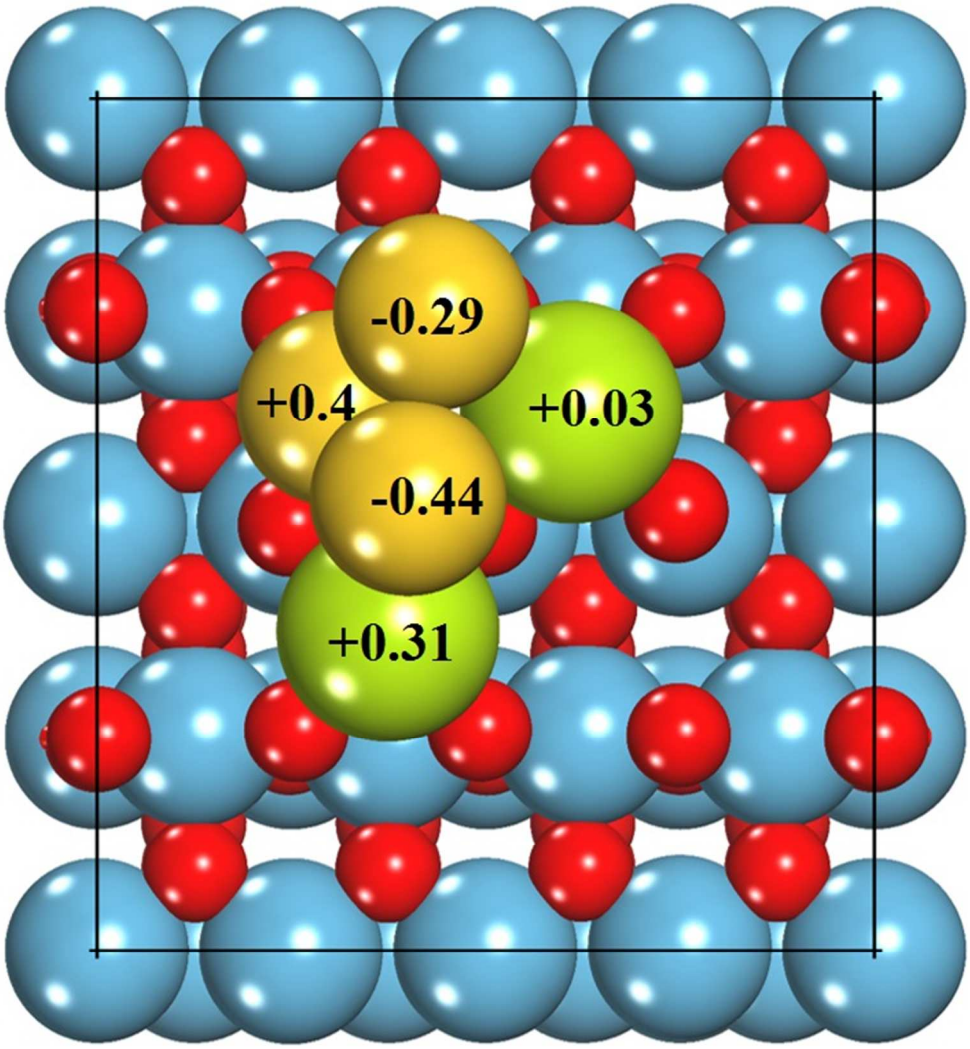

154x164mm (120 x 120 DPI)

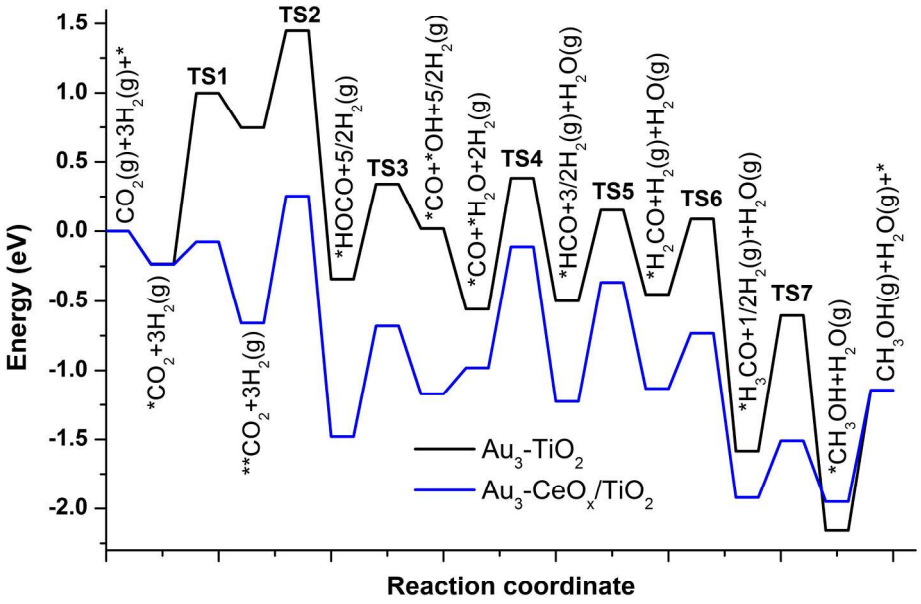

203x153mm (300 x 300 DPI)